J|A|C|S ARTICLES

Published on Web 08/23/2010

Structure of Hydronium (H_3O^+)/Chloride (Cl^-) Contact Ion Pairs in Aqueous Hydrochloric Acid Solution: A Zundel-like Local Configuration

John L. Fulton*,† and Mahalingam Balasubramanian‡

Chemical and Materials Sciences Division, Pacific Northwest National Laboratory, Richland, Washington 99354, and Advanced Photon Source, Argonne National Laboratory, Argonne, Illinois 60439

Received February 18, 2010; E-mail: john.fulton@pnl.gov

Abstract: A comprehensive analysis of the H_3O^+ and H_2O structure in the first solvation shell about Cl^- in aqueous HCl solutions is reported from X-ray absorption fine structure (XAFS) measurements. Results show increasing degree of contact ion pairing between Cl^- and H_3O^+ as the HCl concentration increases from 6.0 m, 10.0 m, and finally 16.1 m HCl (acid concentrations are expressed as molality or mole HCl/1000 g water). At the highest acid concentration there are on average, approximately 1.6 H_3O^+ ions and 4.2 H_2O's in the first shell about Cl^-. The structure of the Cl^-/H_3O^+ contact ion pair is distinctly different from that of the H_2O structure about Cl^-. The Cl−O bond length (2.98 Å) for Cl^-/H_3O^+ is approximately 0.16 Å shorter than the Cl^-/H_2O bond. The bridging proton resides at an intermediate position between Cl and O at 1.60 Å from the Cl^- and approximately 1.37 Å from the O of the H_3O^+. The bridging-proton structure of this contact ion pair, ($Cl-H-OH_2$), is similar to the structure of the water Zundel ion, ($H_2O-H-OH_2^+$). In both cases there is a shortened Cl−O or O−O bond, and the intervening proton bond distances are substantially longer than for the covalent bonds of either HCl or H_2O. A detailed structural analysis of the aqueous chloride species, $Cl^-/(H_2O)_n$, was also completed as part of this study in order to understand the relative importance of various XAFS photoelectron scattering paths. For aqueous Cl^- the measured Cl−O and Cl−H distances of 3.14 Å and 2.23 Å, respectively, are in excellent agreement with earlier neutron and X-ray diffraction results. Overall, these results significantly improve our understanding of the interaction of H_3O^+ with Cl^-. The results are of interest to fundamental physical chemistry and they have important consequences in biochemical, geochemical, and atmospheric processes.

1. Introduction

Hydronium ion (H_3O^+) is one of the most important and ubiquitous species in all aqueous systems, and yet it remains one of the most elusive for direct structural characterization by experimental methods due to its chemical similarity to the primary solvent, water (H_2O). Further, the ion pair species of hydronium with chloride (Cl^-) plays an important role in various aspects of biochemistry, geochemistry, and atmospheric chemistry, but there is as yet no consensus on the structural details. X-ray diffraction (XRD) and neutron diffraction with isotopic substitution (NDIS) have provided many details of the aqueous HCl system from the early major work of Triolo and Narten[1] to the later studies that followed.[2−4] The challenge with these scattering methods is that there are no less than 10 different pair distribution functions that describe the positions of the various, H's, O's, and Cl's in the system.[1] Significant progress has been made in deconvoluting these functions,[2−5] most recently employing Monte Carlo methods with classical potentials. In this report we use X-ray absorption fine structure (XAFS) spectroscopy as a local probe of the pair distribution functions only in the vicinity of the Cl^-. In the XAFS process, a photoelectron is ejected from the 1-s core of Cl to the continuum using an X-ray beam with an energy of ∼2.8 keV. The photoelectron has limited mean free path and an effective scattering contribution that falls off as r^2 from the central absorber. This provides excellent short-range sensitivity. The element-specific nature of the technique coupled with its short-range sensitivity is of advantage to investigate the $Cl^-/H_2O/H_3O^+$ system since only the Cl−H (nearest) and Cl−O pair distributions that are part of the first solvent shell about the halide are probed. Under the assumption that only water and hydronium reside in the Cl^- first shell, this results in essentially four different pair distribution functions, thus greatly simplifying the analysis of the Cl^- solvation. A recent success[6] using XAFS to probe aqueous coordination about Cl^- led to the interesting opportunity to probe the interaction of Cl^- with hydronium.

In dilute acid solutions the HCl is fully dissociated with the hydrated proton likely existing in Eigen (H_3O^+) or Zundel forms

† Pacific Northwest National Laboratory.
‡ Argonne National Laboratory.

(1) Triolo, R.; Narten, A. H. *J. Chem. Phys.* **1975**, *63*, 3624–3631.
(2) Botti, A.; Bruni, F.; Imberti, S.; Ricci, M. A.; Soper, A. K. *J. Chem. Phys.* **2004**, *121*, 7840–7848.
(3) Botti, A.; Bruni, F.; Ricci, M. A.; Soper, A. K. *J. Chem. Phys.* **2006**, *125*, 014508.
(4) Mancinelli, R.; Sodo, A.; Bruni, F.; Ricci, M. A.; Soper, A. K. *J. Phys. Chem. B* **2009**, *113*, 4075–4081.
(5) Agmon, N. *J. Phys. Chem. A* **1998**, *102*, 192–199.
(6) Dang, L. X.; Schenter, G. K.; Glezakou, V. A.; Fulton, J. L. *J. Phys. Chem. B* **2006**, *110*, 23644–23654.

($H_5O_2^+$) solvated by water.[7−10] At higher concentrations solvent-separated ion pairs and contact ion pairs exist between the hydrated proton and the Cl^- anion. Significant progress has been made in understanding these ion pair structures using theoretical methods including studies of small clusters[11−14] and ab initio molecular dynamic simulations of larger systems.[9,15−19] However many questions remain about bond distances and coordination numbers for the pairing of H_3O^+ with Cl^-. XAFS has been especially useful at probing the structure of contact ion pairs between transition metals and halide ions.[20−22] The degree of ion pairing in these systems is strongly promoted at high temperatures where the hydrogen-bonding network in water begins to break down, enhancing the electrostatic attraction between ions. Under ambient conditions, contact ion pairing can often be induced and probed with XAFS at high salt concentrations.[23,24] In the first part of this report we explore, in detail, the structure of water about Cl^-. This provides a basis for completing a comprehensive structural analysis of Cl^-/H_3O^+ in a series of HCl concentrations up to the saturation point.

2. Experimental and Theory Section

2.1. Chemicals and Procedures. Sodium chloride (99.999%), lithium chloride (99.99%) and aqueous, 37 wt % hydrochloric acid having purity of 99.999% on trace metals basis were used as received from Aldrich. Distilled, deionized water was used throughout. Three different acid solutions were examined having molalities (mol/1000 g H_2O) of 6.0, 10.0 16.1 m HCl corresponding to molar HCl:H_2O ratios of 1:9.3, 1:5.6, and 1:3.5, respectively. The later concentration corresponds to the concentrated acid that is 37 wt % HCl in water. Further, 2.5 m NaCl and 15 m LiCl stock solutions were prepared gravimetrically by dissolution of preweighed molar quantities of the salt into 25 g of H_2O.

2.2. XAFS Experimental Methods. The chloride K-edge (2822 eV) XAFS spectra were collected in transmission mode on the bending magnet beamline (PNC/XSD, Sector 20) at the Advanced Photon Source, Argonne National Laboratory. Details of the XAFS beamline methods are given elsewhere.[23,25] The spectra were acquired using transmission pathlengths of 25 μm for the 16.1 m HCl and 15 m LiCl solutions and 75 μm for the 2.5 m NaCl solutions. The samples were contained between two 4 μm thick prolene films that were stretched over 25 or 75 μm thick Kapton spacers. Spectra that were acquired using different path lengths were identical, demonstrating that absorption effects did not distort the $\chi(k)$ data. The absorption edge height, $\Delta\mu_0$, was below 2 in all cases as required to eliminate X-ray leakage effects.

We used portions of the Athena and Artemis programs for the analysis of XAFS data,[26−28] while the theoretical standards were calculated using FEFF8.[29,30] Signal from the atomic background function was removed from the backscattering signal, $\chi(k)$, by setting a Fourier filter distance, R_{bkg}. During fitting, the K-edge XAFS data were weighted by k^3, and windowed between $1.9 < k < 7.8$ Å^{-1} using a Hanning window with $dk = 1.0$ Å^{-1}. The fits were to both the real and imaginary parts of $\tilde{\chi}(R)$ in the region of $0.8 < R < 5.5$ Å. Although all the fitting is done using k^3-weighting, the $|\tilde{\chi}(R)|$ and Im $[\tilde{\chi}(R)]$ plots in the paper are shown with k^2-weighting to better illustrate the higher-order scattering features above 3.5 Å whose origin is from the lower-k region of the $\chi(k)$ plot. In a prior publication, the aqueous first-shell Cl^- coordination number of 6.4 H_2O's was established by comparison to an aqueous standard.[6] In the present study this measured value of the coordination number was adopted, establishing the value of the core hole factor, $S_0^2 = 0.92$. S_0^2 has an associated uncertainty of about 15% that results in an approximate ±15% uncertainty in the reported coordination number. Within FEFF8, the parameter defining the muffin-tin radii overlap for the H's was set to 0.8 as recommended in the FEFF8 documentation.[31] The resulting muffin tin radii for water about chloride were 0.519, 0.959, and 0.952 Å for H, Cl, and O, respectively. Finally the option for automated self-consistent potential calculations (SCF) within FEFF8 was used, providing improved and more consistent estimates of edge energies for all scattering paths.

The atomic background function, $\mu_0(E)$, also contains a series of weak multielectron absorption edges that are not fully removed through Fourier filtering. These features appear in the $\chi(k)$ data at $k = 2.0$, 2.8, and 8.1 Å^{-1} and they correspond to the $KM_{II,III}$, KM_I and $KL_{II,III}$ transitions, respectively. The first two edges only contribute a few percent to the scattering signal at low k and thus have little consequence to the fitted parameters. However, the multielectron edge at 8.1 Å^{-1} was difficult to remove completely and uniformly from all spectra, and hence, the data analysis extended up to the onset of this edge or 7.8 Å^{-1}. Although the k range is relatively short, the primary distances for the water and the hydronium are well resolved.

2.3. XAFS Modeling. Before evaluating the aqueous HCl system we completed a comprehensive evaluation of the water structure about Cl^- for a 2.5 m NaCl solution. This helps provide a clearer picture of the type of information that can be extracted from an XAFS analysis. XAFS studies of aqueous Br^- have provided key insights into the nature of the important photoelectron scattering properties for anion-water systems and these scattering properties are utilized in this study. The importance of Br−H scattering was first recognized in early Br^-/methanol studies by

(7) Xantheas, S. S. *Nature* **2009**, *457*, 673–674.
(8) Marx, D. *ChemPhysChem* **2006**, *7*, 1848–1870.
(9) Buch, V.; Dubrovskiy, A.; Mohamed, F.; Parrinello, M.; Sadlej, J.; Hammerich, A. D.; Devlin, J. P. *J. Phys. Chem. A* **2008**, *112*, 2144–2161.
(10) Swanson, J. M. J.; Maupin, C. M.; Chen, H. N.; Petersen, M. K.; Xu, J. C.; Wu, Y. J.; Voth, G. A. *J. Phys. Chem. B* **2007**, *111*, 4300–4314.
(11) Milet, A.; Struniewicz, C.; Moszynski, R.; Wormer, P. E. S. *J. Chem. Phys.* **2001**, *115*, 349–356.
(12) Struniewicz, C.; Milet, A.; Sadlej, J.; Moszynski, R. *Int. J. Quantum Chem.* **2002**, *90*, 1151–1162.
(13) Ndongmouo, U. F. T.; Lee, M. S.; Rousseau, R.; Baletto, F.; Scandolo, S. *J. Phys. Chem. A* **2007**, *111*, 12810–12815.
(14) Chaban, G. M.; Gerber, R. B.; Janda, K. C. *J. Phys. Chem. A* **2001**, *105*, 8323–8332.
(15) Sillanpaa, A. J.; Laasonen, K. *Phys. Chem. Chem. Phys.* **2004**, *6*, 555–565.
(16) Heuft, J. M.; Meijer, E. J. *Phys. Chem. Chem. Phys.* **2006**, *8*, 3116–3123.
(17) Asthagiri, D.; Pratt, L. R.; Kress, J. D. *Proc. Natl. Acad. Sci. U.S.A.* **2005**, *102*, 6704–6708.
(18) Laasonen, K.; Klein, M. L. *J. Am. Chem. Soc.* **1994**, *116*, 11620–11621.
(19) Wang, F.; Izvekov, S.; Voth, G. A. *J. Am. Chem. Soc.* **2008**, *130*, 3120–3126.
(20) Fulton, J. L.; Chen, Y. S.; Heald, S. M.; Balasubramanian, M. *J. Chem. Phys.* **2006**, *125*, 094507.
(21) Chen, Y. S.; Fulton, J. L.; Partenheimer, W. *J. Am. Chem. Soc.* **2005**, *127*, 14085–14093.
(22) Hoffmann, M. M.; Darab, J. G.; Palmer, B. J.; Fulton, J. L. *J. Phys. Chem. A* **1999**, *103*, 8471–8482.
(23) Fulton, J. L.; Heald, S. M.; Badyal, Y. S.; Simonson, J. M. *J. Phys. Chem. A* **2003**, *107*, 4688–4696.
(24) Chen, Y. S.; Fulton, J. L.; Partenheimer, W. *J. Solution Chem.* **2005**, *34*, 993–1007.
(25) Fulton, J. L.; Linehan, J. C.; Autrey, T.; Balasubramanian, M.; Chen, Y.; Szymczak, N. K. *J. Am. Chem. Soc.* **2007**, *129*, 11936–11949.
(26) Newville, M. *J. Synchrotron Radiat.* **2001**, *8*, 322–324.
(27) Ravel, B.; Newville, M. *J. Synchrotron Radiat.* **2005**, *12*, 537–541.
(28) Stern, E. A.; Newville, M.; Ravel, B.; Yacoby, Y.; Haskel, D. *Physica B* **1995**, *208 & 209*, 117–120.
(29) Zabinsky, S. I.; Rehr, J. J.; Ankudinov, A.; Albers, R. C.; Eller, M. J. *Phys. Rev. B.* **1995**, *52*, 2995–3009.
(30) Rehr, J. J.; Albers, R. C. *Rev. Mod. Phys.* **2000**, *72*, 621–654.
(31) FEFF8 Documentation; http://leonardo.phys.washington.edu/feff/, 2010.

D'Angelo et al.[32] whereas the Br−H−O focusing paths were identified by Simonet et al.[33] and Mayanovic et al.[34] The amplitude of the Br−H−O scattering path is nearly equivalent to that of the Br−O path, and thereby these two signals dominate the total scattering signal. The more recent studies have included contributions from both Br−H and Br−H−O paths.[33,35,36] The FEFF code was updated in 2000 to properly calculate the muffin tin potentials of water[37] although prior studies of aqueous Br^- provided sufficient accuracy to measure the Br−O distance and coordination numbers even in the absence of the various H contributions.[38,39] In our previous study[6] of aqueous Cl^-, we modeled the system with Cl−O, Cl−H−O (3- and 4-leg paths). In this paper we include the Cl−H single scattering in order to determine the Cl−H distances. The Cl−H scattering contribution represents an additional 10% of the total scattering signal. In addition, the Cl−H scattering is decoupled from the various Cl−O scattering paths. This is demonstrated by the fact that the earlier measurements[6] of the Cl−O distance and Debye−Waller factor (3.11 Å and 0.029 Å^2, respectively) are essentially the same as the values reported in this paper.

Figure 1 shows the primary scattering paths, generated from the ab initio scattering code FEFF8, that contribute to the first shell structure. Figure 1 also shows how these scattering signals change as a function of the Cl−H−O angle for water in the first shell. To begin with, in Figure 1a, we see that two scattering paths dominate the overall XAFS signal. These arise from the Cl−O single scattering and the three-leg Cl−H−O multiple scattering paths. To a lesser extent, there is detectable scattering from the four-leg Cl−H−O path. Finally the Cl−H scattering provides a significant addition contribution to the overall scattering, having a much lower frequency oscillation owing to the much shorter bond distance. Note that even using k^3-weighting, the EXAFS signal from H scattering damps out quite rapidly with increasing k values as expected.

The sum of these four scattering paths is used to generate the overall $\chi(k)$. Then this $\chi(k)$ function is Fourier transformed to generate the Im [$\tilde{\chi}(R)$] function of Figure 1b. This Im [$\tilde{\chi}(R)$] function best illustrates the XAFS sensitivity to small changes in the first shell structure. As the Cl−H−O angle is decreased from 180, 165 to 150° there are detectable differences in the scattering functions. There is an R shift that is primarily due to the shortening of the Cl−O distance with smaller angle (the Cl−H distance is fixed in this example). Further, each angle exhibits small but uniquely different changes in the amplitudes of the various peaks in Figure 1b. Hence there is reasonable sensitivity to detect the Cl−H−O angle, φ, about Cl^-. In the fitting process, we used an iterative approach. Starting with $\varphi = 180°$, we determined the Cl−H and Cl−O distances that provided the first guess for the next φ. This iterative approach converged to a least-squares minimization around about 156°. A limitation of this approach is that the Debye−Waller factor does not completely describe the scattering from different Cl−H−O angles in the angular distribution function. The model also assumes that for water the O−H stretch and bending vibrational modes contribute a negligibly small distortion of the O−H bond lengths such that the Debye−Waller Factor for this distance is $\sigma^2 < 0.001$ Å^2.

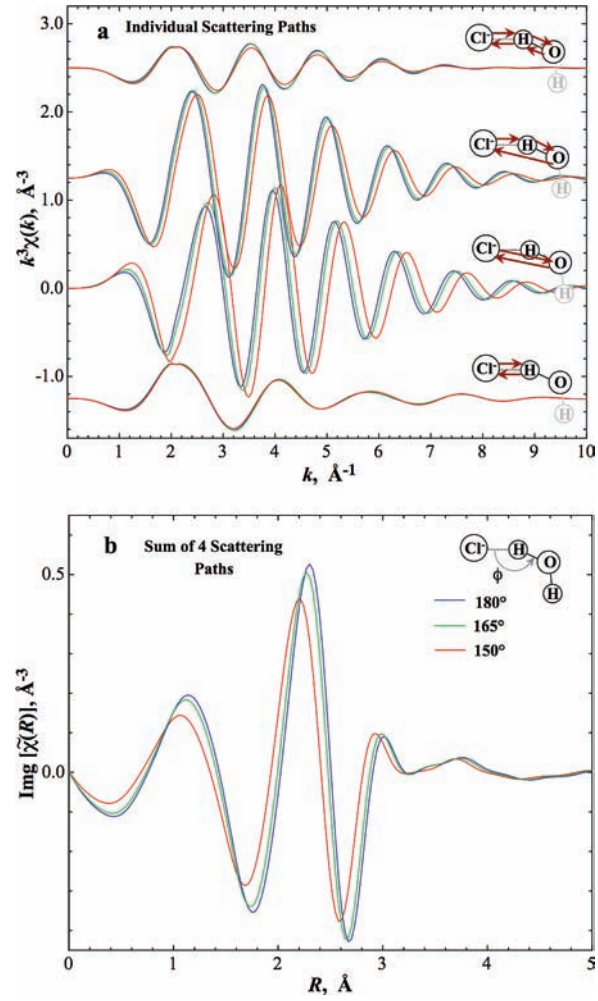

Figure 1. Comparison of (a) k^3-weighted $\chi(k)$ and (b) k^2-weighted Im [$\tilde{\chi}(R)$] plots generated from FEFF8 for H_2O about Cl^- as a function of the Cl−H−O tilt angle (180° (blue), 165° (green), 150° (red)). A k^3-weighting is used in (a) to highlight the high-k oscillations that contribute to the main peak at about 2.5 Å. A k^2-weighting is used in (b) to emphasize the multiple scattering signal above 3.5 Å that originates from lower-k region of the $\chi(k)$ plots. In all cases the scattering parameters were set to the following values, $\sigma^2 = 0.025$ Å^2 and Cl−H distance = 2.23 Å. These values are approximately representative of the experimental values.

In addition to the scattering paths shown in Figure 1, there are higher order scattering contributions that contribute to the $|\tilde{\chi}(R)|$ data in the R region from 3 to 5 Å. These are primarily due to Cl−H−O scattering in which the photoelectron is scattered two or three times between the H−O (low disorder) before return to the Cl. It is necessary to include these contributions to fit the longer R features. Contributions from various inter-H_2O scattering paths (e.g., triangular) are also likely contributors to the scattering in this region.

3. Results and Discussion

3.1. XAFS Spectra for the Aqueous HCl Series. Figure 2a shows the k^3-weighted $\chi(k)$ plots and Figure 2b shows the k^2-weighted $|\tilde{\chi}(R)|$ and Im [$\tilde{\chi}(R)$] plots for a series of HCl solutions from 6.0, 10.0, and 16.1 m HCl. For comparison the spectrum of the fully hydrated Cl^- (2.5 m NaCl) is also given. The k-range is limited to about 8 Å^{-1} due to the existence of a multielectron excitation at 8.1 Å^{-1}. At all acid concentrations there is a significant shift in the oscillations in the $\chi(k)$ plots (Figure 2a), becoming most significant for the 16.1 m HCl. Since the scattering signal is dominated by O scattering, the lower frequency oscillations are a qualitative indication of a shift to

(32) Dangelo, P.; DiNola, A.; Mangoni, M.; Pavel, N. V. *J. Chem. Phys.* **1996**, *104*, 1779–1790.
(33) Simonet, V.; Calzavara, Y.; Hazemann, J. L.; Argoud, R.; Geaymond, O.; Raoux, D. *J. Chem. Phys.* **2002**, *116*, 2997–3006.
(34) Mayanovic, R. A.; Anderson, A. J.; Bassett, W. A.; Chou, I. M. *Chem. Phys. Lett.* **2001**, *336*, 212–218.
(35) Merkling, P. J.; Ayala, R.; Martinez, J. M.; Pappalardo, R. R.; Marcos, E. S. *J. Chem. Phys.* **2003**, *119*, 6647–6654.
(36) D'Angelo, P.; Migliorati, V.; Guidoni, L. *Inorg. Chem.* **2010**, *49*, 4224–4231.
(37) Wilson, K. R.; Tobin, J. G.; Ankudinov, A. L.; Rehr, J. J.; Saykally, R. J. *Phys. Rev. Lett.* **2000**, *85*, 4289–4292.
(38) Wallen, S. L.; Palmer, B. J.; Pfund, D. M.; Fulton, J. L.; Newville, M.; Ma, Y. J.; Stern, E. A. *J. Phys. Chem. A* **1997**, *101*, 9632–9640.
(39) D'Angelo, P.; Di Nola, A.; Filipponi, A.; Pavel, N. V.; Roccatano, D. *J. Chem. Phys.* **1994**, *100*, 985–994.

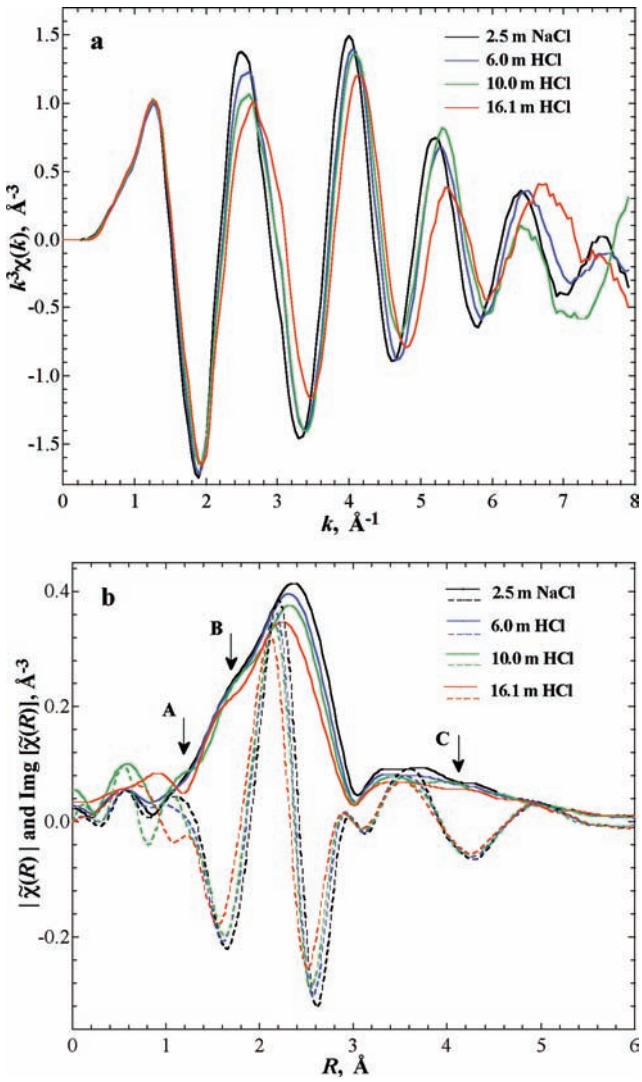

Figure 2. (a) Cl K-edge, k^3-weighted $\chi(k)$ plots for various aqueous Cl^- solutions as indicated. (b) The corresponding k^2-weighted $|\tilde{\chi}(R)|$ (solid lines) and Im $[\tilde{\chi}(R)]$ plots (dashed lines). A k^3-weighting is used in (a) to highlight the high-k oscillations that contribute to the main peak at about 2.5 Å. A k^2-weighting is used in (b) to emphasize the multiple scattering signal above 3.5 Å that originates from lower-k region of the $\chi(k)$ plots.

shorter average Cl−O distances in the HCl solutions. Even at the lowest concentration of this study, 6.0 m HCl, there is a clearly discernible phase shift in the oscillations meaning that the hydrated proton significantly alters the first shell structure at this concentration.

The Fourier transformed spectra shown in Figure 2b are the XAFS representations of the overall Cl−H and Cl−O pair distribution functions. However, using the standard XAFS formalism, the peak positions and shape have not been corrected for the photoelectron amplitude and phase shift functions and as such do not correspond to the true pair distribution functions. The true atom positions and disorder are extracted from fitting to the theoretical standards, and these values are reported in Tables 1 and 2. The primary peak in Figure 2b at about 2.3 Å results from the sum of the three different scattering paths between Cl and the first-shell O. At higher acid concentrations there is a significant contraction of this distance. In addition, there are three significant spectral features marked by the arrows labeled A, B, and C in Figure 2b. Feature "A" is a cusp or reduction in amplitude that appears at approximately 1.3 Å in the $|\tilde{\chi}(R)|$ plot for the most concentrated acid solution. In XAFS, such features are usually associated with a phase cancellation due to "beating" between atoms at slightly different distances. As will be discussed in a later section, this feature is assigned to a shorter Cl−H scattering path that "interferes" with longer Cl−H or Cl−O scattering. The shoulder at feature "B" is due to a combination of Cl−O single scattering and Cl−H−O multiple scattering signals. Finally, the feature "C" is primarily due to longer-range multiple scattering within the Cl−H−O path in which the photoelectron is scattered two or three times between the H−O. It should be noted that the appearance of these three features represented in the $|\tilde{\chi}(R)|$ and Im $[\tilde{\chi}(R)]$ plots will vary slightly depending upon the choice of k range, windowing, and weighting. However by applying the same evaluation range to the theoretical models the recovered fit parameters are mostly independent of these factors. These features are also observed in the spectra of the other halides, Br^- and I^-, as shown in Figure S1 (Supporting Information).

Figure 3 provides an expanded view of the k^2-weighted $|\tilde{\chi}(R)|$ (solid lines) and Im $[\tilde{\chi}(R)]$ plots (dashed lines). A spectrum for 15.0 m LiCl is also included for comparison. The Im $[\tilde{\chi}(R)]$ plot clearly shows the shortening in the average Cl−O for the 16.1 m HCl. In contrast, the water structure about Cl^- for the concentrated LiCl solution shows almost no change in the Cl−O distance but a slight reduction in the amplitude that may be due to displacement of small number of waters by a LiCl contact ion pair. The observation that the water structure about Cl^- in 15.0 m LiCl is nearly the same as for dilute Cl^- agrees with the X-ray and neutron diffraction studies of concentrated LiCl solution by Narten et al.[1,40] This observation supports the premise for the 16.1 m HCl solution, that the hydrating *waters* are not affected by formation of the ion pair but that the contraction in the average Cl−O distance occurs through the formation of a short Cl−O distance associated with the Cl^-/H_3O^+ ion pair.

3.2. XANES Spectra. Figure 4 shows XANES plots for the series of HCl solutions from 6.0, 10.0, and 16.1 m HCl. For comparison a plot for the fully hydrated Cl^- is also included. The spectra are remarkable in their similarity, a clear indication that not only are the coordination numbers and chemical identity of nearest neighbors (H's and O's) largely unchanged, but also that the atoms and ordering of longer range structure (esp. the second shell) are not largely different since the XANES region just beyond the absorption edge is also sensitive to backscattering contributions from this longer range structure.[41] The near-edge region from approximately 2820 to 2828 eV is sensitive to the angular momentum projected unoccupied density of states of the Cl. For comparison the XANES spectra of gaseous HCl is shown. The intense band at 2823 eV for the Cl 1s→3p is a distinct feature of the H−Cl σ bond. Similar intense transitions are reported for Cl−C− bonds.[41] Thus, for the concentrated acid solution, the Cl^- appears to retain its purely ionic state even in the presence of nearby H_3O^+ ions. Evidently, if there is charge transfer from Cl^- to an H^+ in the first shell, then this would occur through overall delocalization of charge about Cl^- rather than through the highly localized charge transfer of a covalent bond.

3.3. Structure of Aqueous Cl^-. The water structure about Cl^- was a subject of a previous XAFS study.[6] In this section we provide a more comprehensive analysis of aqueous Cl^- that moves somewhat beyond that earlier analysis. These results

(40) Narten, A. H.; Vaslow, F.; Levy, H. A. *J. Chem. Phys.* **1973**, *58*, 5017–5023.

Table 1. Structural Parameters from XAFS Fits for Aqueous Cl^- First-Shell Structure under Ambient Conditions

		structure						
system	scatterer	N	R,[b] Å	$\sigma^2 \times 10^3$,[b] Å^2	$\sigma^2_{ClOH} \times 10^3$,[a,b] Å^2	$\sigma^2_{MS} \times 10^3$,[a,b] Å^2	φ Cl−H−O, deg	$\mathscr{R}$[c]
2.5 m NaCl	H_{H_2O}	6.4[d]	2.234(0.041)	30.1(7.6)				0.011
	O_{H_2O}	6.4[d]	3.143(0.015)	24.3(2.1)	40.0(10.6)	24.9(17.3)	156	

[a] The subscripts ClOH, and MS refer to 3-leg Cl−H−O paths and higher-order Cl−H−O paths, respectively. For the 4-leg, Cl−H−O path, the Debye−Waller factor is set to the value for the Cl−H path. [b] The uncertainties correspond to an increase in the misfit (defined by a sum of squares) between the data and the best-fit model by an amount of $1/\nu$, where ν is the degrees of freedom in the fit (ref 28). [c] Goodness of fit defined by a scaled sum of squares as described in FEFFIT. [d] Fixed to value derived from various aqueous and crystalline standards.[6]

Table 2. Structural Parameters from XAFS Fits for Aqueous HCl First-Shell Structure under Ambient Conditions. Two Different Structural Models are Applied, One Involving Just Two Oxygen Shells and a Second with Two Different H and O Shells

		structure					
system	scatterer	N[b]	R,[b] Å	$\sigma^2 \times 10^3$,[b] Å^2	$\sigma_{ClOH}{}^2 \times 10^3$,[a,b] Å^2	$\sigma_{MS}{}^2 \times 10^3$,[a] Å^2	$\mathscr{R}$[c]
16.1 m HCl	O_{H_2O}	4.6(1.0)	3.133(0.019)	27.3(14.8)	27.3(14.8)[e]		0.061
	$O_{H_3O^+}$	1.0[d]	2.965(0.039)	13.3(5.4)	13.3(5.4)[e]		
16.1 m HCl	H_{H_2O}	4.2(0.5)	2.234[f]	30.1[f]			0.038
	O_{H_2O}	4.2(0.5)	3.143[f]	24.3[f]	40.0	24.9	
	$H_{H_3O^+}$	1.6(0.3)	1.604(0.041)	24.6(9.9)			
	$O_{H_3O^+}$	1.6(0.3)	2.975(0.014)	15.9(3.1)	15.9(3.1)[e]		

[a] The subscripts ClOH, and MS refer to 3-leg Cl−H−O paths and higher order Cl−H−O paths, respectively. [b] The uncertainties correspond to an increase in the misfit (defined by a sum of squares) between the data and the best-fit model by an amount of $1/\nu$, where ν is the degrees of freedom in the fit (ref 28). [c] Goodness of fit defined by a scaled sum of squares as described in FEFFIT. [d] Fixed in the fitting. [e] For this model, the Debye−Waller factors for 2-leg Cl−O, 3-leg, and 4 leg Cl−H−O paths were equivalent. The higher-order scattering paths were not fit in this case. [f] Fixed in the fitting to the values for aqueous Cl^-.

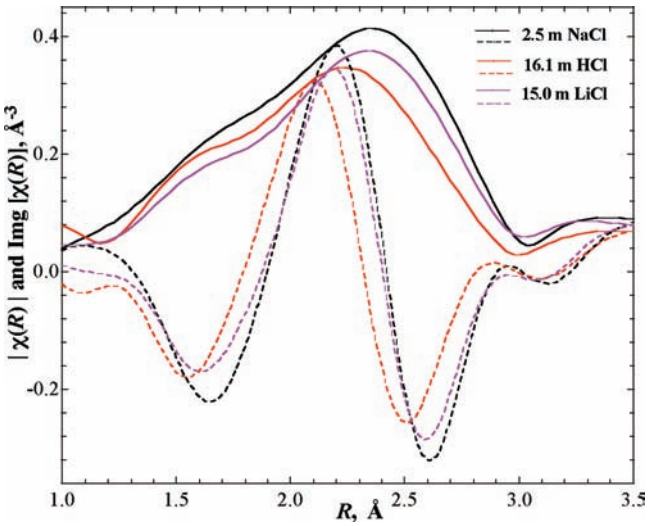

Figure 3. Expanded view of the k^2-weighted $|\tilde{\chi}(R)|$ (solid lines) and Im $[\tilde{\chi}(R)]$ (dashed lines) plots for 2.5 m NaCl, 16.1 m HCl and, for comparison, the spectrum for 15.0 m LiCl.

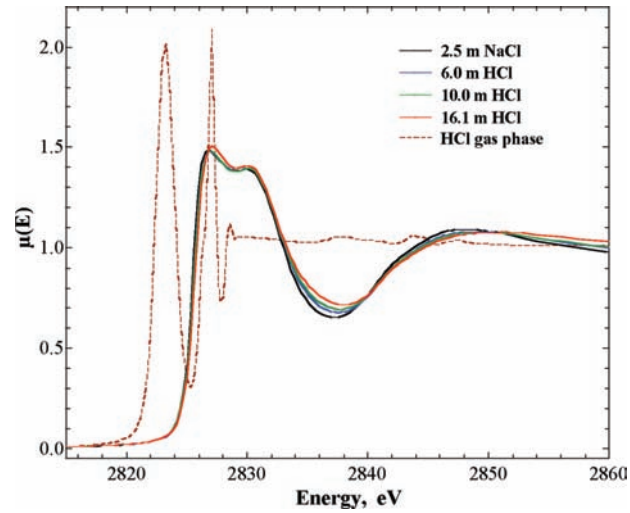

Figure 4. Series of XANES spectra, $\mu(E)$, for various aqueous HCl and an NaCl solutions as shown. For comparison, the $\mu(E)$ spectrum of gas-phase HCl is also shown.

illustrate the sensitivity of XAFS to various structural features of the first hydration shell and thus provide a basis for analysis of the Cl^-/H_3O^+ system that follows. Figure 5 shows the results of fitting the theoretical standards (FEFF8) to the experimental data to extract the structural parameters for the 2.5 m NaCl solution that are reported in Table 1. The contributions to the total $\chi(k)$ from each of the theoretical scattering paths are shown in Figure S3 (Supporting Information). The Cl−H and Cl−O distances of 2.23 and 3.14 Å are in excellent agreement with values derived from the NDIS study by Powell et al.[42] of 2.28 and 3.1 Å, respectively. From XAFS, the Debye−Waller factor (the bond distance disorder) for Cl−H and Cl−O are $\sigma^2 = 0.030$ and 0.024 Å^2, respectively, wherein the Cl−H bond distance shows slightly more disorder than for the Cl−O bond. From Powell's NDIS results[42] the Debye−Waller factors for Cl−H and Cl−O are 0.027 and 0.022 Å^2, respectively. (These NDIS values are derived from the reported full-widths-at-half-maximum of the first peaks in the corresponding pair distribution functions.) Again these Debye−Waller factors are in good agreement with the XAFS results including the somewhat greater disorder in the C−H versus Cl−O bond distances. Finally, the fitted Cl−H−O angle of 156° shows that the H-bonding to the Cl occurs primarily through a single proton and that the water dipole moment is partially aligned with the Cl in an orientation that also allows for hydrogen bonding between waters in the first and second shells. (The angle Cl−H−O φ is calculated via the approximation that the motions of Cl−H and Cl−O are not correlated[42−44]).

(41) Myneni, S. C. B. *Science* **2002**, *295*, 1039–1041.
(42) Powell, D. H.; Neilson, G. W.; Enderby, J. E. *J. Phys.: Condens. Matter* **1993**, *5*, 5723–5730.

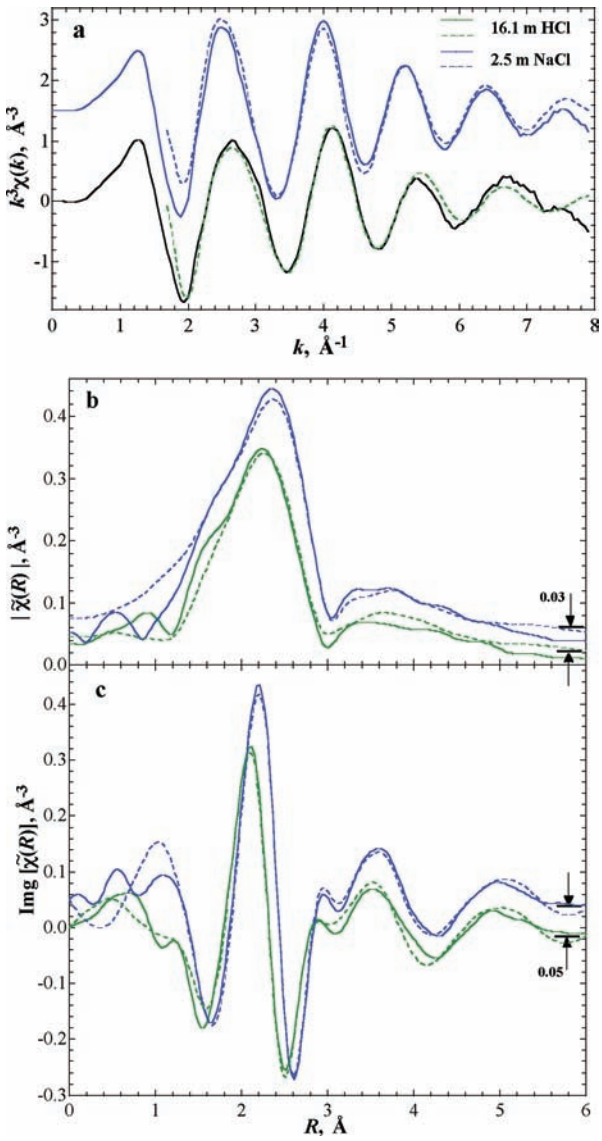

Figure 5. Results of fitting the Cl K-edge spectra for the 2.5 m NaCl and 16.1 m HCl solutions to FEFF8 structure models in (a) k^3-weighted $\chi(k)$ plots, (b) k^2-weighted $|\tilde{\chi}(R)|$ and (c) Im $[\tilde{\chi}(R)]$ plots. The experimental data (solid lines) and the model fit (dashed lines) are shown. The fitted lines are results from the FEFF8 standards using the parameters listed in Tables 1 and 2. A k^3-weighting is used in (a) to highlight the high-k oscillations that contribute to the main peak at about 2.5 Å. A k^2-weighting is used in (b) and (c) to emphasize the multiple scattering signal above 3.5 Å that originates from lower-k region of the $\chi(k)$ plots. The two sets of spectra have been offset as indicated for clarity.

3.4. Structure of the Aqueous HCl Solutions. Three different strategies were employed in fitting the XAFS spectrum for 16.1 m HCl solution. Initially, an attempt was made to fit the scattering data using a single Cl−O distance. This result showed a contraction in the average Cl−O distance but a complete failure to reproduce (not shown) the dominant features of the $\chi(k)$ and $|\tilde{\chi}(R)|$ spectra. The second approach involved a fit using two different Cl−O distances. These results are reported as the first set of fitted parameters listed in Table 2. In this case, there is a new short Cl−O distance at 2.96 Å that is assigned to the contact ion pair between the Cl^- and the H_3O^+. Further the Debye−Waller factor is significantly lower ($\sigma^2 = 0.013$ Å^2) for the H_3O^+ species than for water ($\sigma^2 = 0.030$ Å^2), indicating the much stronger binding of this ion pair species. There is also a second Cl−O distance at 3.13 Å that has a Debye−Waller factor of $\sigma^2 = 0.027$ Å^2. This distance is assigned to water molecules in the first shell. Both the distance and the disorder are nearly identical to the values measured for the fully hydrated Cl^- reported in Table 1. In agreement with the XRD data of Triolo[1] for the concentrated HCl acid, their $g_{Cl-O}(r)$ plot shows a strong feature at 3.13 Å that was assigned to the Cl−O distance of water about Cl^-.

These findings led to the adoption of the third model in order to achieve the best refinement of the H_3O^+ structural parameters. In this case the water structural parameters were fixed to their values for the aqueous Cl^- species and subsequently, the structural parameters for H_3O^+ and the coordination numbers for both H_3O^+ and H_2O were fit. These results are shown as the second set of parameter entries in Table 2, in the fitted curves in Figure 5 and in the schematic of Figure 6. The contributions to the total $\chi(k)$ from each of the theoretical scattering paths are shown in Figure S7 (Supporting Information). Notably, a short Cl−H distance of 1.60 Å is detected that is associated with the hydronium proton. The O of that hydronium is located at a Cl−O distance of 2.98 Å. As in the case of scattering from water (Figure 1), the bridging proton provides a focusing effect that leads to 3- and 4-leg scattering paths. This aspect helps to confirm the location of this proton with respect to the O of H_3O^+. The Debye−Waller factor for the Cl−H distance is $\sigma^2 = 0.025$ Å^2, a value that is only slightly less than the Cl−H disorder for water. In contrast the disorder of the O of the H_3O^+ is quite small, $\sigma^2 = 0.016$ Å^2 with respect to that for H_2O of 0.030 Å^2. This suggests that the potential well for the bridging proton is quite broad, while that for the O on the H_3O^+ is quite narrow. The Debye−Waller factor for this Cl−H bond is much larger than would be expected for a Cl−H covalent bond of undissociated HCl.

In XAFS spectroscopy, detecting scattering from an H atom is generally a challenging problem since the electron number (1) is typically much lower than that for nearby atoms such as O (8). In certain circumstances it is possible to detect the H atom scattering when the distances are short and the disorder is relatively low. The hydronium H atom is particularly well located about Cl^- for the strongest possible H scattering. First, the very short Cl−H distance (1.60 Å) clearly differentiates this distance from all other nearby atoms (H and O) from a spatial resolution point of view. The shorter distance also significantly enhances the scattering amplitude with respect to the H atoms of water at 2.23 Å. Finally the Debye−Waller factor is somewhat lower for the H atom on the H_3O^+. The combination of these last two factors leads to a scattering intensity from the single H of H_3O^+, that is about 5 times more intense than scattering from one H on the water. Hence, there is a strong scattering signal from the proton of the hydronium. In the strictest sense, an H^+ or proton has no photoelectron scattering cross section due to absence of an electron. However, by charge transfer from an adjoining Cl^- or from other hydrogens on the hydronium ion, a localized electron about the H atom will contribute to the scattering. A "proton", or H atom without an electron, is a convenient entity for chemical definition but in water it exists only perhaps in a brief transition state.

Table 2 also reports the fitted coordination numbers for both H_3O^+ and H_2O about Cl^-. For H_3O^+ the coordination number

(43) Powell, D. H.; Neilson, G. W. *J. Phys.: Condens. Matter* **1990**, *2*, 3871–3878.
(44) Szasz, G. I.; Dietz, W.; Heinzinger, K.; Palinkas, G.; Radnai, T. *Chem. Phys. Lett.* **1982**, *92*, 388–392.

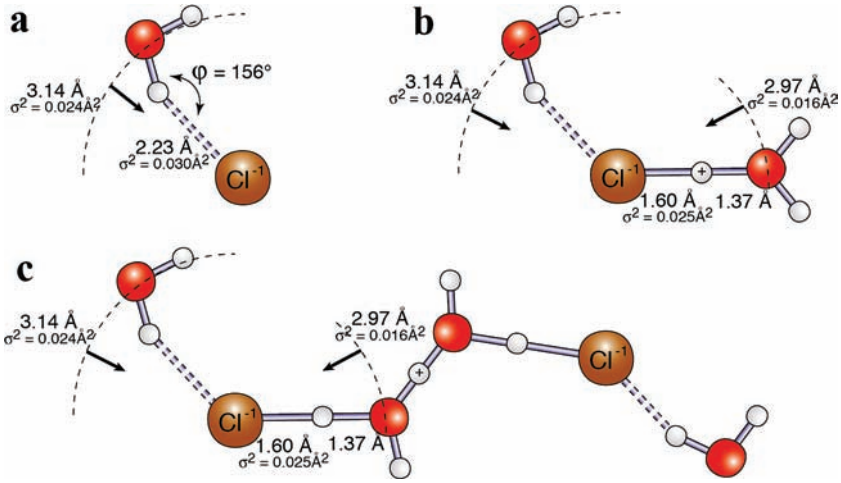

Figure 6. Schematic of the H_2O and H_3O^+ or $H_5O_2^+$ structure about Cl^- from fitting of XAFS spectra for (a) 2.5 m NaCl in water, (b) 16.1 m HCl in water (Eigen model), (c) 16.1 m HCl in water (Zundel model). For clarity, only one of the waters and hydronium ions about chloride are illustrated.

is 1.6. This suggests that significantly more than one H_3O^+ is paired with each Cl^-. In order to maintain the 1:1 stoichiometry of H^+/Cl^- this would mean that an Eigen species is frequently paired with more than one Cl^- or that a water Zundel ion bridges two Cl^- as shown in the schematic of Figure 6c. The measured water coordination number is 4.2 giving a total coordination about Cl of 5.8 ± 0.8.

The H_3O^+ coordination number about Cl^- was also estimated for the two lower HCl concentration solutions having 6 and 10 m HCl. At lower concentrations, the sensitivity for measuring the Cl^-/H_3O^+ structural parameters is significantly reduced. Thus, a simple approximation was used involving a linear combination of the Cl^-/H_3O^+ and Cl^-/H_2O structures that were derived from the 16.1 m HCl solution. The XAFS data was fit by starting with two different fixed representations (FEFF8) for the bond distances and Debye−Waller factors of the H_3O^+ and H_2O. The H_3O^+/H_2O coordination number ratio was then fitted while setting the total Cl^- coordination to 5.8. This model returns Cl^-/H_3O^+ coordination numbers of 0.7 (±0.2) and 1.0 (±0.3) for the 6.0 and 10.0 m solutions, respectively. This shows that a significant amount of contact ion pairing occurs even at 6 m HCl for these monovalent ions. The presence of solvent-separated ion pairs would not be detected by XAFS because second shell species are too disordered. However the fact that we detect approximately one Cl^-/H_3O^+ contact ion pair suggests that the solvent-separated ion pair is less important at these concentrations. The overall H_3O^+/Cl^- ratio is 1, whereas for these more dilute systems the likelihood of having a Cl^- bridging H_3O^+ species is less likely. Hence the fact that we detect approximately one contact ion pair implies that the solvent-separated ion pairs are less likely.

3.5. Details of the Cl^-/H_3O^+ Ion Pair Structure. The structural details of the Cl^-/H_3O^+ ion pair are summarized in the schematic of Figure 6. Many of the structural features of this Cl^-/H_3O^+ ion pair, in which a proton bridges the O and Cl atoms, are similar to the structural aspects of a Zundel ion ($H_5O_2^+$) in which the two O atoms are bridged by a proton. The Cl−O distance for the ion pair is 0.17 Å shorter than the Cl−O distance for water hydrogen bonded to Cl^-. Likewise the Zundel ion has an O−O distance of 2.4 Å that is significantly shorter than O−O distance of 2.85 Å between hydrogen-bonded water molecules.[17,45] In the Zundel ion ($H_2O-H-OH_2^+$), the bridging proton is asymmetrically located between the O's at distances of 1.15 to 1.35 Å. These distances are 0.2 to 0.4 Å longer than the O−H bond of a water molecule. Likewise the Cl−H (1.60 Å) and O−H (1.37 Å) bond distances for the ion pair ($Cl-H-OH_2$) are 0.35 and 0.40 Å longer than for their covalent analogues of HCl (gas phase) and H_2O, respectively. (By assuming that the Cl−H−O bond is collinear, the calculated O−H bond distance is then 1.37 Å).

These new experimental results for the local structure about Cl^- in aqueous HCl solutions are substantially different than previous experimental studies of aqueous phase solutions. The clearest departure from the earlier analyses are the short Cl−O and Cl−H distances for the Cl^-/H_3O^+ contact ion pair. However, the two sets of Cl−O and Cl−H distances measured from XAFS are consistent with a series of peaks in the $g(r)$ functions for Cl−O and Cl−H that have been reported in earlier scattering experiments. The earlier XRD $g(r)$ data (sensitive to the Cl−O and O−O distances) from Triolo[1] for 13.9 m HCl, show a primary peak at 3.13 Å and a shoulder on this peak at approximately 2.9−3.0 Å that are consistent with the XAFS assignments of Cl−O distances for water (3.14 Å) and hydronium (2.98 Å), respectively. The 2.9−3.0 Å shoulder was not specifically noted by Triolo but was later deconvolved by Agmon.[5] The earlier NDIS g(r) results[1] (sensitive to the Cl−H, O−H distances) show strong features at distances of 2.1 Å and 1.6 Å (previously assigned to only O−H distances) that are consistent with the XAFS assignments for Cl−H distances for water (2.23 Å) and hydronium (1.60 Å), respectively. Thus these new XAFS findings regarding the Cl^-/H_3O^+ structure do not contradict the earlier scattering results. The most recent NDIS results by Mancinelli et al.[4] use empirical potentials in a Monte Carlo refinement to recover the 10 different pair distribution functions of the HCl acid solution. In that study, the reported Cl−O distance for the Cl^-/H_3O^+ contact ion pair was ~2.85 Å with a Cl−H distance of 1.85 Å. The results again confirm the short Cl−O bond for the H_3O^+ although the Cl−H distance is considerably longer than from the XAFS measurement.

Many of the features of the measured Cl^-/H_3O^+ species are captured by first principles calculations for both small clusters

(45) Coskuner, O.; Jarvis, E. A. A.; Allison, T. C. *Angew. Chem., Int. Ed.* **2007**, *46*, 7853–7855.

and for larger systems modeled using molecular dynamics simulations. Small clusters of up to six water molecules often provide key insights into the bulk phase structure.[6] Cluster calculation (CCSD(T)/B3LYP) by Milet et al.[11] for a 5 H_2O + 1 HCl cluster, show Eigen and Zundel species bonding to Cl^- wherein the Cl−O distances of the hydrated proton species lie between 2.8−2.9 Å while adjoining water molecules hydrogen-bond to the Cl with Cl−O distance of 3.15−3.25 Å. Various optimized cluster geometries show the Cl−H distances between 1.41 and 1.8 Å, whereas the O−H distances for this bridging proton are between 1.1−1.4 Å. Both bonds are substantially longer than the corresponding covalent bonds within HCl and H_2O. These features are in excellent agreement with the XAFS results. Similar results for small clusters have been reported by Devlin[46] and Ndongmouo[13] (MP2 and DFT-BLYP).

The ab initio molecular dynamics study (DFT/BLYP/DZVP) by Buch[9] illustrates the bimodal nature of the bridging-proton position for various HCl-hydrates. This concept of a bimodal state is further exemplified by the bridging proton position of dissociated and undissociated forms of HCl in small clusters. For small $HCl:(H_2O)_n$ clusters ($n < 4$) the HCl does not dissociate. At approximately 4 waters the ionic form begins to become more stable.[11] Finite temperature significantly affects the equilibrium where higher temperatures favor the undissociated form[13] while the presence of additional nearby Cl^-'s appears to help favor the ionic form.[14] The H−Cl bond length for the undissociated acid in a small cluster, $(HCl)_4{\bullet}(H_2O)_4$ is 0.06 Å longer than that for the isolated HCl molecule.[14] Addition of one or two water molecules hydrogen-bonding to the HCl appears to further elongate the "undissociated" HCl bond to about 1.4 Å.[11,46] From the XAFS measurements the water coordination number is 4.2 so that these additional hydrating waters would presumably lead to further lengthening of the H−Cl bond of any "undissociated" acid. Further from small cluster calculations the *dissociated* proton resides at approximately 1.7 to 1.85 Å.[11,46] From the XAFS measurements, the disorder for the H−Cl bond is much higher than for the Cl−O bond and this leads to a possible conclusion that the bridging proton exist in two states between an elongated, "undissociated" HCl bond ($Cl-H\cdots OH_2$) and that of the fully dissociated form ($Cl\cdots H-OH_2$).

The first principles molecular dynamics simulations (DFT/BLYP) of Sillanpää et al.[15] capture a Cl−O distance of 3.0 and 3.2 Å for the hydronium and water, respectively, in good agreement with the XAFS results. The corresponding Cl−H distances of 2.1 and 2.4 Å for the hydronium and water, respectively, are both substantially longer than for the XAFS results. They also report a Cl−H distance of 1.35 Å assigned to a covalent bond in the $Cl-D-Cl^-$ ion. This proton position is substantially shorter than the value measured by XAFS that is assigned to the Cl^-/H_3O^+ ion pair. Their reported $g_{Cl-Cl}(r)$ shows a very disordered Cl−Cl peak at about 4 Å that would not be detected by XAFS. The existence of the $Cl-D-Cl^-$ ion species cannot be confirmed by XAFS. Finally, there are the molecular dynamics simulations (DFT/BLYP) of Heuft et al.[16] that produce Cl−O distances of 3.15 and 2.97 Å for the water and hydronium, respectively, while reporting a Cl−H distance of 1.95 for the hydronium. Again the Cl−O distances are in agreement with the XAFS results, while the Cl−H for the hydronium is substantially longer. In the future it would be very interesting to benchmark ab initio simulation results directly to the XAFS spectra via the MD-XAFS approach.[6,47] As a final note, the Lennard-Jones intermolecular potentials that are used in classical molecular dynamics simulations mostly use Cl^-/H_3O^+ interaction parameters that are derived from mixing rules and thus fail to capture the specific structure of the Cl^-/H_3O^+ interaction.

Conclusions

Photoelectron scattering in the XAFS process probes the local structure about Cl and thus provides important new insights into the structure in concentrated HCl solutions and compliments X-ray and neutron scattering methods that probe the overall structure of the solution. As a result, a comprehensive new view of the hydronium (H_3O^+)/ chloride (Cl^-) ion pair structure is reported. This XAFS study shows that, at the lowest concentration of the study (6 m HCl), the Cl^-/H_3O^+ ion pair is starting to form in appreciable amounts up to the point in the concentrated acid (16 m HCl) where all of the H_3O^+ species are paired with a Cl^-. The hydronium ion in the first shell resides at a distance that is about 0.16 Å shorter than the nearby water molecules, whereas the proton that bridges the Cl^- and the H_3O^+ is shifted even closer to the Cl^- to a Cl−H distance of 1.6 Å. In many respects this bridged proton structure of the ion pair, ($Cl-H-OH_2$), is similar to that for the Zundel ion, ($H_2O-H-OH_2^+$). The highest level of ab initio theory for small clusters provides good agreement with most of the experimentally observed structures. On the other hand ab initio-based molecular dynamics simulations capture some but not all of the measured local structure. Finally the Cl^-/H_3O^+ ion pair structure may be difficult to reproduce using classical intermolecular potentials or models that rely on these potentials.

Acknowledgment. This work was supported by the U.S. Department of Energy's (DOE) Office of Basic Energy Sciences, Division of Chemical Sciences, Geosciences and Biosciences. PNNL is operated for the Department of Energy by Battelle. PNC/XSD facilities at the Advanced Photon Source, and research at these facilities, are supported by the U.S. Department of Energy - Basic Energy Sciences, a major facilities access grant from NSERC, the University of Washington, Simon Fraser University, the Pacific Northwest National Laboratory, and the Advanced Photon Source. Use of the Advanced Photon Source is also supported by the U.S. Department of Energy, Office of Science, Office of Basic Energy Sciences, under Contract DE-AC02-06CH11357.

Supporting Information Available: XAFS spectra and analysis. This material is available free of charge via the Internet at http://pubs.acs.org

JA1014458

(46) Devlin, J. P.; Uras, N.; Sadlej, J.; Buch, V. *Nature* **2002**, *417*, 269–271.

(47) Palmer, B. J.; Pfund, D. M.; Fulton, J. L. *J. Phys. Chem.* **1996**, *100*, 13393–13398.